ISSN 0915-633X

NATIONAL INSTITUTE FOR FUSION SCIENCE

On the Stability of Mercier and Ballooning Modes in Stellarator Configurations

C.C. Hegna and N. Nakajima

(Received - Aug. 22, 1997)

NIFS-510 Oct. 1997

This report was prepared as a preprint of work performed as a collaboration reserch of the National Institute for Fusion Science (NIFS) of Japan. This document is intended for infomation only and for future publication in a journal after some rearrangements of its contents.

Inquiries about copyright and reproduction should be addressed to the Research Information Center, National Institute for Fusion Science, Oroshi-cho, Toki-shi, Gifu-ken 509-02 Japan.

RESEARCH REPORT
NIFS Series

NAGOYA, JAPAN

On the Stability of Mercier and Ballooning Modes in Stellarator Configurations

C. C. Hegna[†] and N. Nakajima

National Institute for Fusion Science

Nagoya, Japan 464-01

[†]*Departments of Engineering Physics and Physics*

University of Wisconsin, Madison, WI 53706-1687 USA

Key words: ballooning modes, Mercier criterion, Stellarators

Abstract

The stability properties of pressure driven ballooning and Mercier modes in general stellarator configurations are studied. A method originally introduced to study tokamak stability by J. M. Greene and M. S. Chance [Nucl. Fusion **21**, 453 (1981)] is generalized to three-dimensional systems. This method introduces a way to examine various stability physics mechanisms by using a perturbation theory. Variations in equilibrium quantities are introduced to a localized region whose amplitude is small but whose cross field derivative is large. Consistent with this ordering, changes in the magnetic coordinates and metric elements are calculated using Boozer coordinates. In the general case, the set of equilibria are characterized by two free functions, which are usually chosen to be the local variation of pressure and rotational transform profiles. In this way, a stability space for Mercier and ballooning modes is generated which is parameterized by the average shear and pressure gradient at the magnetic surface of interest. If an additional currentless constraint is imposed, the change in the local rotational transform profile and the local pressure gradient are related; in this limit only

one free function parameterizes the set of equilibria. A different way to view the stability information is plot the stability curves in a space parameterized by the local pressure gradient and the field-line-averaged parallel current. When viewed using these plots, it's possible to show that a second stability regime always exists for Mercier modes at sufficiently large pressure gradient.

Pac. Nos. 52.35.Py, 52.55.Hc, 52.55.Dy

I. Introduction

As the confinement properties of stellarator configurations improve with increased understanding and improved design, the question of beta limits in stellarators becomes an issue. Since most stellarators operate with little or no equilibrium current, kink and tearing modes are not expected to limit performance. Therefore, criteria for ballooning and Mercier stability are often used to predict the stability limits in these configurations. While little experimental evidence exists in stellarator experiments to justify this,[1] a variety of high performance tokamak experiments have shown that marginal stability properties of ballooning modes determine the pressure profile over extensive portions of the plasma cross-section.[2,3] In this work, we examine the fundamental ideal magnetohydrodynamic (MHD) equations involved in predicting Mercier and ballooning stability. A useful analysis tool will be introduced which can be used to develop insights into the nature of stellarator stability, and hopefully provide some intuition into improving the stability properties of helical systems.

In general, the stability properties of equilibria to ideal MHD modes are obtained by numerically solving a partial differential equation. Considerable simplicity is found by considering localized modes with large wavelength.[4,5] In this limit, the stability properties are described by an ordinary differential equation, the ballooning equation, which locally can also be applied to general three-dimensional geometries.[6] Mercier stability is determined from an analytically derived criterion which can be obtained from the asymptotic properties of the ballooning equation.[7]

For stellarator configurations, it was suspected that as long as the average magnetic shear, as measured by the gradient of the rotational transform, was positive ($d\iota/d\psi > 0$), ballooning modes would be stable as long as Mercier

stability was satisfied.[8] A counter-example to this thesis was found in a Heliac configuration.[9] This result can be explained by noting that the Pfirsch-Schlüter current effects can change the flux surface averaged magnetic shear and cause ballooning instability in the $d\iota/d\psi < 0$ region.[10] However, additional numerical calculations of the ballooning equations have also uncovered ballooning instabilities in the positive shear region of stellarators which is in direct conflict with the Shafarnov conjecture.[11]

Since the ballooning eigenmode equation has a rather simple structure, it is useful to examine this equation to discover the various physical mechanisms at work. Several aspects of ballooning modes in tokamak configurations were clarified by using an interesting approach for generating a class of related equilibria.[12] In Greene and Chance,[12] (denoted GC for the rest of this paper), additional small amplitude, short length scale variations in various quantities are imposed on an initial arbitrary MHD equilibrium. The variations are constrained such that the resultant state is also an equilibrium. The GC technique allows for the independent variation of the gradients of the pressure and safety factor, so that their impact on ballooning stability can be studied separately. One result of this work was showing the importance of the local shear in ballooning stability. In particular, the appearance of the second regime of ballooning stability was shown to be present due to the movement of the point of small local shear from the bad curvature region towards the good curvature region as the pressure induced variation of the local shear increases.

In this work, we generalize the calculations of GC to three-dimensional equilibria. As in GC, the local shear plays an important role in determining the ballooning stability properties. In addition, the effects of flux-surface-averaged parallel currents and curvature can also be quantified. Recent studies have been carried out with a similar goal in mind, to get a good physical feel for the

underlying ideal MHD stability properties of stellarator configurations.[13-15] The advantage of the present approach is that the stability properties of any equilibrium can be explained without invoking the stellarator expansion or assuming small aspect ratio, small plasma beta, or weak shaping. In principle, this approach could then be used to study any class of stellarator configuration, and can be used to augment the various ideal MHD stability studies that have been performed for particular configurations.[16-21]

A significant difference between the ballooning stability of stellarators and tokamaks is in the spectrum.[14,22,23] In systems with a continuous symmetry, such as a tokamak, the ballooning mode eigenvalues are characterized by the flux surface label, ψ, and the radial wave number θ_k, and are independent of the field line label α. In general three-dimensional equilibria, the eigenvalues are α dependent, and therefore the structure of the eigenfunction in the (ψ,θ_k,α) space may be much different from the analogous eigenfunction of tokamak-like equilibria. In particular, the level surfaces of the eigenvalues for tokamaks are topological cylinders in the (ψ,θ_k,α) space, whereas the level surfaces of the eigenvalues for stellarators can be spherical in this space due to the strong α dependence. It is suggested that the technique introduced here can be used to clarify in what region of parameter space the distinct topological structures may be important.

In the following section, the Boozer coordinate system[24] will be introduced to describe the MHD equilibrium quantities. Using this coordinate system, the GC technique will be used to generate a class of equilibria that are parameterized, in the general case, by two free functions. Mercier stability for these equilibria are determined in Section III. In Section IV, the ballooning equation for this class of equilibria is derived. In Section V, the special limit of stellarator equilibrium is considered where the flux-surface-averaged current is

taken to be zero. In this limit, an additional constraint is imposed on the equilibria variations, so that only one free function parameterizes the set of equilibria. A concluding discussion is given in Section VI.

II. MHD Equilibrium

In this section, we characterize the MHD equilibrium using Boozer coordinates. We assume the existence of three dimensional equilibria with a set of nested flux surfaces. Whether such equilibria exists or not is still an open theoretical question which we will not address here. In particular, we view the problem of resonant denominators as an issue of an ill-defined equilibrium that can be resolved by introducing magnetic islands.[25]

A. Boozer Coordinates

Boozer coordinates[24] allow the magnetic field to be expressed in both a covariant and contravariant basis set of the variables (ψ,θ,ζ), which are respectively, the toroidal flux function, the poloidal angle and toroidal angle. The magnetic field is written

$$\mathbf{B} = \nabla\psi \times \nabla(\theta - \iota\zeta) \ , \tag{1}$$

$$\mathbf{B} = J\nabla\zeta + I\nabla\theta + \beta\nabla\psi \ , \tag{2}$$

where ι is the rotational transform, and J and I are flux functions. The function $J(\psi)$ is proportional to the amount of poloidal current flowing outside the flux surface ψ, while $I(\psi)$ is proportional to the amount of toroidal current located within flux surface ψ. The function β is a function of all three magnetic coordinates in general, and is related to the Pfirsch-Schlüter currents. The Jacobian of this coordinate system is related to the spectrum of the magnetic field strength by the relation

$$\sqrt{g} = (\nabla\psi\times\nabla\theta\cdot\nabla\zeta)^{-1} = \frac{J+\iota I}{B^2}$$

$$= V'(\psi)[1 + \sum_{mn}{}' \delta_{mn} e^{im\theta - in\zeta}] \quad , \tag{3}$$

where $V'(\psi) = \oint dl/B$, $(2\pi)^2 V(\psi)$ is the volume enclosed by the flux surface and the sum excludes (m,n) = (0,0).

Since equations (1) and (2) must represent the same magnetic field, the conditions

$$J = \frac{g_{\zeta\zeta} + \iota g_{\zeta\theta}}{\sqrt{g}} \quad , \tag{4}$$

$$I = \frac{g_{\zeta\theta} + \iota g_{\theta\theta}}{\sqrt{g}} \quad , \tag{5}$$

$$\beta = \frac{g_{\zeta\psi} + \iota g_{\theta\psi}}{\sqrt{g}} \quad , \tag{6}$$

must be satisfied, where the metric elements $g_{ij} = \partial \mathbf{x}/\partial\varphi_i \cdot \partial \mathbf{x}/\partial\varphi_j$ are constructed from the inverse mapping of the magnetic coordinates $\mathbf{x} = \mathbf{x}(\psi,\theta,\zeta)$, where $\varphi \in (\psi,\theta,\zeta)$.

The MHD equilibrium condition $J \times \mathbf{B} = \nabla p$ is given by

$$-J' - \iota I' + (\frac{\partial}{\partial\zeta} + \iota\frac{\partial}{\partial\theta})\beta = p'\sqrt{g} \quad , \tag{7}$$

where the prime refers to the derivative with respect to the function's argument. The flux surface average of Eq. (7) yields the relation $J' + \iota I' = -p'V'$ which is essentially a description of the diamagnetic current. The term β can be written as a Fourier expansion. The elements of the expansion are related to the magnetic field spectrum by $\beta_{mn} = p'V'\delta_{mn}/i(m\iota - n)$. An additional useful expression is that for the parallel current

$$\frac{\mathbf{J}\cdot\mathbf{B}}{B^2} = \sigma - p'V'\lambda \quad , \tag{8}$$

where σ is the flux-surface-averaged net parallel current and is related to I by

$$\sigma = I' + \frac{p'V'I}{J + \iota I} \quad , \tag{9}$$

and λ is a measure of the Pfirsch-Schlüter current spectrum

$$\lambda = \sum_{mn}{}' \lambda_{mn} e^{im\theta - in\zeta} \quad , \tag{10}$$

where the Fourier coefficients are related to the magnetic field spectrum by

$$\lambda_{mn} = \delta_{mn} \frac{mJ + nI}{(m\iota - n)(J + \iota I)} \quad , \tag{11}$$

which is derived from the condition $p'V'\lambda = (\mathbf{B} \times \nabla\psi \cdot \nabla\beta)/B^2$.

B. Generation of Equilibria

We now proceed by considering variations in the plasma quantities imposed on some given initial arbitrary equilibrium. The initial equilibrium satisfies Eqs. (1)-(10), with the profiles denoted $p^{(0)}(\psi)$, $\iota^{(0)}(\psi)$, $\sigma^{(0)}(\psi)$, $J^{(0)}(\psi)$, $I^{(0)}(\psi)$, and $\beta^{(0)}(\psi,\theta,\zeta)$ and coordinates defined by $\mathbf{x}^{(0)}(\psi,\theta,\zeta)$. Since Mercier and ballooning stability are determined by the local values of the pressure gradient, shear, etc., it's useful to construct these variations localized to a particular magnetic surface of interest. Following GC, we consider variations in the parameters which are small, but whose cross-field gradients are large. All quantities will be expressed in terms of the magnetic coordinates of the initial equilibrium, but since the magnetic field is allowed to vary, these coordinates are not the magnetic coordinates of the perturbed magnetic field. In what follows, we will write the variations in the inverse coordinate mapping, but we show in the Appendix how this is related to the associated magnetic coordinate variation.

The pressure profile is then described in the vicinity of the magnetic surface ψ_b by the expansion

$$p(\psi) = p^{(0)}(\psi) + \mu p^{(1)}(y) + \ldots \tag{12}$$

where $y = (\psi - \psi_b)/\mu$, and $\mu << 1$ is the expansion parameter. Notice that $dp/d\psi = p^{(0)'} + p^{(1)'}$ has an order unity variation although the variation of the pressure amplitude itself is small. In a similar way, we expand the functions

$$\iota(\psi) = \iota^{(0)}(\psi) + \mu\iota^{(1)}(y) + \ldots \tag{13}$$

$$J(\psi) = J^{(0)}(\psi) + \mu J^{(1)}(y) + \ldots \tag{14}$$

$$I(\psi) = I^{(0)}(\psi) + \mu I^{(1)}(y) + \ldots \tag{15}$$

To be consistent with MHD force balance, it is required that the function β have order unity corrections caused by the equilibrium variations. An appropriate expansion is given by

$$\beta(\psi,\theta,\zeta) = \beta^{(0)}(\psi,\theta,\zeta) + \beta^{(1)}(y,\theta,\zeta) + O(\mu) \ldots \tag{16}$$

The coordinate mapping is also perturbed and written

$$\mathbf{x}(\psi,\theta,\zeta) = \mathbf{x}^{(0)}(\psi,\theta,\zeta) + \mu\mathbf{x}^{(1)}(y,\theta,\zeta) + \ldots \ . \tag{17}$$

From Eq. (17), the metric elements

$$g_{\zeta\zeta} = g_{\zeta\zeta}^{(0)} + O(\mu) \ , \tag{18}$$

$$g_{\zeta\theta} = g_{\zeta\theta}^{(0)} + O(\mu) \ , \tag{19}$$

$$g_{\theta\theta} = g_{\theta\theta}^{(0)} + O(\mu) \ , \tag{20}$$

are unaffected to lowest order, but the metric elements

$$g_{\zeta\psi} = g_{\zeta\psi}^{(0)} + \frac{\partial \mathbf{x}^{(0)}}{\partial\zeta}\cdot\frac{\partial \mathbf{x}^{(1)}}{\partial y} + O(\mu) \ , \tag{21}$$

$$g_{\theta\psi} = g_{\theta\psi}^{(0)} + \frac{\partial \mathbf{x}^{(0)}}{\partial\theta}\cdot\frac{\partial \mathbf{x}^{(1)}}{\partial y} + O(\mu) \ , \tag{22}$$

$$g_{\psi\psi} = g_{\psi\psi}^{(0)} + 2\frac{\partial \mathbf{x}^{(0)}}{\partial \psi}\cdot\frac{\partial \mathbf{x}^{(1)}}{\partial y} + \frac{\partial \mathbf{x}^{(1)}}{\partial y}\cdot\frac{\partial \mathbf{x}^{(1)}}{\partial y} + O(\mu) \ , \tag{23}$$

have order unity corrections due to the variations.

The induced variations are constrained so that the profiles in (12)-(17) also describe the equilibrium. In addition, the variation is assumed to keep the value of the magnetic field strength fixed to lowest order in μ, so that at the magnetic surface under scrutiny the magnetic spectrum as given by (3) is undisturbed. The condition of MHD force balance, Eq. (7) leads to the conditions

$$J^{(1)\prime} + \iota^{(0)} I^{(1)\prime} = -p^{(1)} V' \ , \tag{24}$$

$$\left(\frac{\partial}{\partial \zeta} + \iota^{(0)}\frac{\partial}{\partial \theta}\right)\beta^{(1)} = p^{(1)\prime}(\sqrt{g} - V') \ , \tag{25}$$

where V' and $\sqrt{g}$ are the initial equilibrium values. Equations (24) and (25) describe the additional diamagnetic and Pfirsch-Schlüter currents generated from the pressure variation. Clearly, $\beta^{(1)}$ is given by a Fourier expansion whose components are given by $\beta_{mn}^{(1)} = p^{(1)} V' \delta_{mn} / i(m\iota^{(0)} - n)$ which is analogous to the same expression for $\beta^{(0)}$ in terms of $p^{(0)\prime}$ and the magnetic field spectrum.

The condition that the magnetic field strength is undisturbed to lowest order is given by the condition

$$\frac{\partial \mathbf{x}^{(1)}}{\partial y}\cdot\frac{\partial \mathbf{x}^{(0)}}{\partial \theta} \times \frac{\partial \mathbf{x}^{(0)}}{\partial \zeta} = \frac{\partial \mathbf{x}^{(1)}}{\partial y}\cdot\nabla\psi \sqrt{g} = 0 \ , \tag{26}$$

which implies $\partial \mathbf{x}^{(1)}/\partial y$ can be written

$$\frac{\partial \mathbf{x}^{(1)}}{\partial y} = C\mathbf{B} + D\frac{\mathbf{B} \times \nabla\psi}{B^2} \ , \tag{27}$$

where C and D are yet to be determined. Equation (6) has order unity corrections due to the variations, which can be written $\beta^{(1)} = \mathbf{B}^{(0)}\cdot(\partial \mathbf{x}^{(1)}/\partial y)$. This leads to the condition

$$C = \frac{\beta^{(1)}}{B^2} \quad . \tag{28}$$

Since C and $\beta^{(1)}$ are proportional to $p^{(1)\prime}$, the variation in $\mathbf{x}^{(1)}$ along **B** can be obtained by integrating up the fast variation. A similar procedure can be used to find the cross field variation once an expression for D is obtained.

The final constraints are obtained from the corrections in Eqs. (4) and (5). To lowest order these two equations are unaffected by the variations, but since the derivatives of J and I enter into the force balance relation, it's also important that the ψ-derivatives of (4) and (5) are also satisfied. A linear combination of the derivatives of (4) and (5) leads to the condition

$$\begin{aligned} 0 = {} & \sqrt{g}(I^{(0)}J^{(1)\prime} - J^{(0)}I^{(1)\prime}) + \iota^{(1)\prime}(J^{(0)}g^{(0)}_{\theta\theta} - I^{(0)}g^{(0)}_{\theta\zeta}) \\ & + J^{(0)}\left(\frac{\partial \mathbf{x}^{(0)}}{\partial\zeta}\cdot\frac{\partial}{\partial\theta}\frac{\partial \mathbf{x}^{(1)}}{\partial y} + \frac{\partial \mathbf{x}^{(0)}}{\partial\theta}\cdot\frac{\partial}{\partial\zeta}\frac{\partial \mathbf{x}^{(1)}}{\partial y} + 2\iota^{(0)}\frac{\partial \mathbf{x}^{(0)}}{\partial\theta}\cdot\frac{\partial}{\partial\theta}\frac{\partial \mathbf{x}^{(1)}}{\partial y}\right) \\ & - I^{(0)}\left(\iota^{(0)}\frac{\partial \mathbf{x}^{(0)}}{\partial\zeta}\cdot\frac{\partial}{\partial\theta}\frac{\partial \mathbf{x}^{(1)}}{\partial y} + \iota^{(0)}\frac{\partial \mathbf{x}^{(0)}}{\partial\theta}\cdot\frac{\partial}{\partial\zeta}\frac{\partial \mathbf{x}^{(1)}}{\partial y} + 2\frac{\partial \mathbf{x}^{(0)}}{\partial\zeta}\cdot\frac{\partial}{\partial\zeta}\frac{\partial \mathbf{x}^{(1)}}{\partial y}\right) . \end{aligned} \tag{29}$$

By using (24), (27) and (28), Eq. (29) can be simplified to yield a relationship involving D and $\iota^{(1)\prime}$,

$$0 = \iota^{(1)\prime} + \left(\frac{\partial}{\partial\zeta} + \iota\frac{\partial}{\partial\theta}\right)D + \frac{1}{g^{\psi\psi}}\left(J\frac{\partial}{\partial\theta} - I\frac{\partial}{\partial\zeta}\right)\beta^{(1)} - \frac{J + \iota I}{g^{\psi\psi}}I^{(1)\prime} - \frac{IV'}{g^{\psi\psi}}p^{(1)\prime} \quad , \tag{30}$$

where $g^{\psi\psi} = \nabla\psi\cdot\nabla\psi$, and unless otherwise explicitly specified, all the terms are given in terms of the initial equilibrium. We introduce the notation

$$\oint Q \equiv \oint \frac{d\theta}{2\pi}\oint \frac{d\zeta}{2\pi}Q \ , \tag{31}$$

to define the flux surface average of any quantity Q. By applying the averaging operator to (30), a constraint equation involving the rotational transform gradient is derived.

$$0 = \iota^{(1)\prime} - I^{(1)\prime}(J + \iota I)\oint \frac{1}{g^{\psi\psi}} - p^{(1)\prime} IV' \oint \frac{1}{g^{\psi\psi}} + p^{(1)\prime} V'(J + \iota I)\oint \frac{\lambda}{g^{\psi\psi}} \quad (32)$$

where the Pfirsch-Schlüter coefficient λ as defined in Eqs. (10)-(11) has been used. Equation (32) can also be written

$$0 = \iota^{(1)\prime} - \sigma^{(1)}(J + \iota I)\oint \frac{1}{g^{\psi\psi}} + p^{(1)\prime}(J + \iota I)\oint \frac{\lambda}{g^{\psi\psi}} , \quad (33)$$

by using Eq. (9) to identify the variation in the net parallel current. In the limit of zero net current, (33) shows that the rotational transform gradient is affected by the combination of Pfirsch-Schlüter currents and noncircularity. This is essentially the same physics that was pointed out in Ref. (10). Using Eq. (32) to substitute for $I^{(1)\prime}$ in (30), an equation for D is derived:

$$\left(\frac{\partial}{\partial\zeta} + \iota\frac{\partial}{\partial\theta}\right)D = \iota^{(1)\prime}\frac{1}{\oint \frac{1}{g^{\psi\psi}}}\left(\frac{1}{g^{\psi\psi}} - \oint \frac{1}{g^{\psi\psi}}\right)$$

$$- p^{(1)\prime}\frac{V'(J+\iota I)}{\oint \frac{1}{g^{\psi\psi}}}\left(\frac{\lambda}{g^{\psi\psi}}\oint \frac{1}{g^{\psi\psi}} - \frac{1}{g^{\psi\psi}}\oint \frac{\lambda}{g^{\psi\psi}}\right) , \quad (34)$$

which describes the coordinate variation D in terms of the functions $\iota^{(1)\prime}$ and $p^{(1)\prime}$.

In summary the eight function variations, (12)-(17) are constrained by six conditions, given by Eqs. (24)-(26), (28), (32), and (34) where C and D are defined by Eq. (27). In this way, the set of equilibria produced by these variations are classified by two free functions which are typically taken to be $p^{(1)\prime}$ and $\iota^{(1)\prime}$. In the following sections, we will classify the stability of these equilibria by considering the two free variations independently. Another potentially useful choice for the two functions is $p^{(1)\prime}$ and $\sigma^{(1)}$ where the average current is substituted for the average shear. By this choice one is able to address the issue of stability in currentless stellarators. This will be discussed in Sec. V.

III. Mercier Stability

Mercier stability is determined by the quantity

$$D_I = E + F + H - \frac{1}{4}, \tag{35}$$

where $D_I > 0$ indicates instability and E, F, and H are defined in Ref. (26). The various quantities in (35) can be evaluated in the perturbed equilibria. Using $p^{(1)\prime}$ and $\iota^{(1)\prime}$ to classify the equilibrium variations, Mercier stability is determined by

$$D_I = -\frac{p^{(0)\prime} + p^{(1)\prime}}{(\iota^{(0)\prime} + \iota^{(1)\prime})^2} V\dagger\dagger - \frac{1}{4}, \tag{36}$$

where

$$V\dagger\dagger = (J + \iota I)[V'' \oint \frac{1}{g^{\psi\psi}} + \iota V' \oint \frac{\lambda}{g^{\psi\psi}}]$$

$$- p'[V'(J + \iota I)]^2 \{\oint \frac{\lambda^2}{g^{\psi\psi}} \oint \frac{1}{g^{\psi\psi}} - (\oint \frac{\lambda}{g^{\psi\psi}})^2 + \oint \frac{1}{g^{\psi\psi}} \oint \frac{g}{[V'(J+\iota I)]^2}\} \tag{37}$$

is a function of the initial equilibrium only. The Mercier stability boundary is given by a parabola in the p'-ι' parameter space. If $V\dagger\dagger < 0$, the unstable region lies where $p' > 0$. The case where $V\dagger\dagger > 0$ is shown in Figure 1 which shows the larger the magnitude of the average shear the larger the allowable pressure gradient for a Mercier stable plasma. Another way to write (36) is by writing it as a function of the Mercier stability index of the initial unperturbed equilibrium, $D_I^{(0)}$,

$$D_I = \frac{p^{(0)\prime} + p^{(1)\prime}}{p^{(1)\prime}} \frac{\iota^{(1)\prime 2}}{(\iota^{(0)\prime} + \iota^{(1)\prime})^2} (D_I^{(0)} + \frac{1}{4}) - \frac{1}{4}, \tag{38}$$

which shows that the condition $V\dagger\dagger > 0$ (< 0) corresponds to $D_I^{(0)} > -0.25$ (< -0.25).

IV. Ballooning Equation

The ballooning equation describes the stability properties of short wavelength modes. In the incompressible limit, this is given by

$$\mathbf{B}\cdot\nabla\frac{|k_\perp|^2}{B^2}\mathbf{B}\cdot\nabla\xi + \frac{2}{B^4}(\mathbf{B}\times\mathbf{k}_\perp\cdot\kappa)(\mathbf{B}\times\mathbf{k}_\perp\cdot\nabla p)\xi + \frac{\rho}{B^2}\omega^2|k_\perp|^2\xi = 0 , \qquad (39)$$

where κ is the magnetic field curvature vector and ρ is the mass density. By writing the curvature vector as

$$\kappa = \kappa_n\nabla\psi + \kappa_g\frac{\mathbf{B}\times\nabla\psi}{g^{\psi\psi}} , \qquad (40)$$

and defining the local shear

$$s \equiv \sqrt{g}\,\frac{\mathbf{B}\times\nabla\psi}{g^{\psi\psi}}\cdot\nabla\times\frac{\mathbf{B}\times\nabla\psi}{g^{\psi\psi}} , \qquad (41)$$

and transforming the angle variables to $\alpha = \theta - \iota\zeta$, $\eta = \zeta$, so that

$$\mathbf{B}\cdot\nabla = \frac{1}{\sqrt{g}}\frac{\partial}{\partial\eta} , \qquad (42)$$

the ballooning mode equation can be written in Boozer coordinates as

$$\frac{\partial}{\partial\eta}\left(\frac{B^2}{g^{\psi\psi}} + g^{\psi\psi}L^2\right)\frac{\partial\xi}{\partial\eta} + 2p'\sqrt{g}\,(J + \iota I)(\kappa_n + \kappa_g L)\xi$$

$$+ \omega^2\rho g\left(\frac{B^2}{g^{\psi\psi}} + g^{\psi\psi}L^2\right)\xi = 0 , \qquad (43)$$

where L is related to the local shear by the integral

$$L(\eta) = \int_{\eta_k}^{\eta} d\eta'\, s(\eta') , \qquad (44)$$

with η_k playing the dual role of an angle-like position where the integrated local shear is chosen to vanish and as a measure of the radial wave vector.[22]

In Boozer coordinates, the curvature components are given by

$$\kappa_n = \frac{1}{B^2}\frac{\partial}{\partial\psi}\left(\frac{B^2}{2}+p\right) + \frac{\beta}{2\sqrt{g}(J+\iota I)}\frac{\partial\sqrt{g}}{\partial\eta}$$

$$+ \frac{Jg_{\psi\theta} - Ig_{\psi\zeta}}{\sqrt{g}g^{\psi\psi}}\frac{J\dfrac{\partial\sqrt{g}}{\partial\theta} - I\dfrac{\partial\sqrt{g}}{\partial\zeta}}{2\sqrt{g}(J+\iota I)} \quad , \tag{45}$$

$$\kappa_g = \frac{I\dfrac{\partial\sqrt{g}}{\partial\zeta} - J\dfrac{\partial\sqrt{g}}{\partial\theta}}{2\sqrt{g}(J+\iota I)} \quad . \tag{46}$$

The local shear has two components given by

$$s = \iota' + \frac{\partial}{\partial\eta}\frac{Jg_{\psi\theta} - Ig_{\psi\zeta}}{\sqrt{g}g^{\psi\psi}} \quad , \tag{47}$$

where the first term is the average shear, while the second term varies on a flux surface and is annihilated by averaging over a field line.

The stability properties of the mode is determined from the competition between the stabilizing field line bending term, given by the first term in (43), and the potential destabilizing pressure/curvature drive of the second term in (43). Ballooning instability occurs when Eq. (43) has a negative eigenvalue, $\omega^2 < 0$. In general, the eigenvalue and eigenmode are functions of ψ,θ_k and the field line label α.

We will now consider the effects of the equilibrium variations on the ballooning mode coefficients. Since we'll be interested in determining the ballooning stability boundary $\omega^2 = 0$, the term containing the eigenvalue will be ignored in what follows. It can be shown that self-consistent variations in the equilibrium leave κ_n, κ_g and $g^{\psi\psi}$ unaffected to lowest order and therefore are given by their values in the initial equilibrium. Additionally, B^2,$\sqrt{g}$, J, I and ι are all undisturbed to lowest order in the variation as previously discussed.

The only place that a variation in the ballooning coefficients occurs is in the local shear and the coefficient of the curvature terms. Namely, the p' explicitly written in (43) is given by $p^{(0)\prime} + p^{(1)\prime}$. The local shear in the presence of the equilibrium variations is given by

$$s = s^{(0)} + s^{(1)} = \iota^{(0)\prime} + \frac{\partial}{\partial\eta}\left(\frac{Jg_{\psi\theta} - Ig_{\psi\zeta}}{\sqrt{g}g^{\psi\psi}}\right) + \iota^{(1)\prime} + \frac{\partial D}{\partial\eta} , \tag{48}$$

where the first two terms are given by the initial equilibrium and $\iota^{(1)\prime}$ and $\partial D/\partial\eta$ describe the effect of changes in the equilibrium with D given in (34). The marginal stability ballooning equation for this set of equilibrium is given by

$$\frac{\partial}{\partial\eta}\left(\frac{B^2}{g^{\psi\psi}} + g^{\psi\psi}L^2\right)\frac{\partial\xi}{\partial\eta} + 2(p^{(0)\prime} + p^{(1)\prime})\sqrt{g}(J + \iota I)(\kappa_n + \kappa_g L)\xi = 0 , \tag{49}$$

where

$$L = (\iota^{(0)\prime} + \iota^{(1)\prime})(\eta - \eta_k) + \frac{Jg_{\psi\theta} - Ig_{\psi\zeta}}{\sqrt{g}g^{\psi\psi}} + D , \tag{50}$$

with the integration constant of D chosen such that $D(\eta_k) = 0$, and the value $\eta = \eta_k$ corresponds to $L(\eta_k) = 0$.

One can now map out the regions of stability and instability in a space parameterized by p' and ι' as was done in Figure 1 for Mercier stability by numerically solving Eq. (49) for a given equilibrium and accounting for the variations through $p^{(1)\prime}$, $\iota^{(1)\prime}$ and D. This was done in GC, to derive the s-α stability curves used to interpret tokamak ballooning stability.

As pointed out in GC, the variation in the local shear plays an important role in determining the stability properties. For analytic insight into the nature of variations of the local shear in stellarators, we introduce a simple analytic representation of the field strength variation and the variation in $g^{\psi\psi}$. In particular, it is assumed that the field strength variation is dominated by a single Fourier harmonic,

$$\sqrt{g} \cong V'[1 + \delta_{mn}\cos(m\theta - n\zeta) + ...] , \tag{51}$$

which produces a Pfirsch-Schlüter coefficient given by

$$\lambda \cong \frac{mJ + nI}{J + \iota I} \frac{\delta_{mn}}{m\iota - n}\cos(m\theta - n\zeta) . \tag{52}$$

Without loss of generality, δ_{mn} is taken to be positive. Additionally, it is assumed that the variation in the noncircularity is dominated by two Fourier harmonics, one of which corresponds to the harmonic of the field strength variation. Specifically, we write

$$\frac{1}{g^{\psi\psi}} \cong G(\psi)[1 - \varepsilon_\psi\cos(m\theta - n\zeta) - \varepsilon_3\cos(m'\theta - n'\zeta) + ...] , \tag{53}$$

where $m'/n' \neq m/n$ and $G(\psi) > 0$. A reasonable assumption is that $1 > \varepsilon_\psi > 0$. This corresponds to a bulging of the flux surfaces into the low field region, for m = 1, a helical shift of the column to the low field side, for m = 2, an elliptic surface that bulges into the low field region, etc. The sign of ε_3 is irrelevant since a redefinition of the angle coordinates can always be chosen that leaves $m\theta - n\zeta$ unchanged but shifts $m'\theta - n'\zeta$ by π. The variation in the local shear induced by the equilibrium variations as given in Eq. (48) is given by

$$\frac{\partial D}{\partial \eta} = -\iota^{(1)\prime}[\varepsilon_\psi\cos(m\theta - n\zeta) + \varepsilon_3\cos(m'\theta - n'\zeta)]$$

$$- p^{(1)\prime}V'G(mJ + nI)\frac{}{m\iota - n}\delta_{mn}[H_o(m\theta - n\zeta) + \varepsilon_3\cos(m'\theta - n'\zeta)H_1(m\theta - n\zeta)] , \tag{54}$$

where H_o and H_1 are functions of the dominant magnetic harmonic $m\theta - n\zeta$ given by

$$H_o(m\theta - n\zeta) = (1 - \frac{\varepsilon_\psi^2}{2})\cos(m\theta - n\zeta) - \frac{\varepsilon_\psi}{2}\cos(2m\theta - 2n\zeta) , \tag{55}$$

$$H_1(m\theta - n\zeta) = \frac{\varepsilon_\psi}{2} + \cos(m\theta - n\zeta) . \tag{56}$$

The limit of a symmetric system can be examined by taking $\varepsilon_3 \Rightarrow 0$. Additionally, we assume $m\theta - n\zeta \cong 0$ is the local bad curvature region which is consistent with Eq. (51). Since ballooning mode eigenfunctions tend to peak in the regions of small local shear, understanding the behavior of D with increasing pressure gradient can yield insight into the physics of ballooning stability. In this limit, the pressure modulation of the local shear enhances the local shear, as described in Eq. (48), in the bad curvature region if $m\iota > n$ and reduces the local shear if $m\iota < n$. In the tokamak limit where $m\iota > n$ and $\iota' < 0$, the pressure modulation at small enough pressure gradient tends to keep the region of small local shear in the bad curvature region.[12] As pressure increases further the small local shear region migrates away from the bad curvature region. As pointed out in GC, this is the reason for the second ballooning stability region of tokamak configurations. For a helically symmetric equilibrium with $n > m\iota$, the situation is completely analogous to the tokamak case if $\iota' > 0$: at low pressure the region of local shear is in the bad curvature region and at higher pressure gradient, the local shear region moves toward the good curvature region. For this reason, we should expect a second stability ballooning region for helically systems with favorable Mercier properties and $\iota' > 0$. Crudely, the properties of a helically symmetric system can be related to the analogous tokamak case by replacing the safety factor q of the tokamak with $1/(\iota - n/m)$ and q'/q with $\iota'/(n/m - \iota)$. It has been noted that the transport properties of helical systems can be calculated by the same procedure.[27] This safety factor transition factor accounts for the reduction of the connection length in helical symmetry. The region of ballooning instability in a perfectly helically symmetric, Mercier stable configuration is in the $\iota' > 0$ region for $n\iota > m$.

From Eq. (53), the three-dimensional effect is destabilizing. With $\varepsilon_3 \neq 0$, an additional field line dependence is introduced into the ballooning coefficients.

For this reason, the ballooning mode eigenfunction becomes field line dependent and is afforded a greater range in space to find regions of small local shear. As discussed previously, the structure of the eigenmode is greatly complicated in three-dimensional configurations[22] and a numerical calculation of the ballooning equation is needed to identify regions of stability.

V. Currentless plasmas

If we limit the class of equilibria under investigation to those without any net parallel current, the set of equilibria is only parameterized by one function. To see this, consider the constraint equation (33) in the limit $\sigma^{(1)} = 0$,

$$\iota^{(1)\prime} = -Ap^{(1)\prime} \quad , \tag{57}$$

where A is a function of the initial equilibrium only

$$A = (J + \iota I) \oint \frac{\lambda}{g^{\psi\psi}} \, . \tag{58}$$

The intersection of Eq. (57) and the stability plots in the two-dimensional parameter space represents the stability properties of currentless stellarators. For the case of Mercier stability, there are two classes of stability solutions. These solutions are characterized by a function of the initial equilibrium G, defined by

$$G = -\frac{4p^{(0)\prime}V^{\iota\iota}}{A^2} - \frac{4\iota^{(0)\prime}V^{\iota\iota}}{A^3} + \frac{4V^{\iota\iota 2}}{A^4} \tag{59}$$

where A is given by Eq. (58). If $G < 0$, there is no Mercier unstable region for any value of pressure gradient at $\sigma^{(1)} = 0$. This is represented by the top line drawn in Figure 1. If $G > 0$, then there exists an unstable region for pressure gradients in the range

$$-\frac{\iota^{(0)\prime}}{A} + \frac{2V^{\iota\iota}}{A^2} - \sqrt{G} < -p^{(1)\prime} < -\frac{\iota^{(0)\prime}}{A} + \frac{2V^{\iota\iota}}{A^2} + \sqrt{G} \, . \tag{60}$$

However as shown by the bottom line in Figure 1, there always exists a second stability region at sufficiently large pressure gradient.

The sign of A is determined by the flux surface average of the noncircularity and the Pfirsch-Schlüter spectrum. In the particular limit described by Eqs. (51)-(53),

$$A \cong -\frac{JG}{2}\,\frac{\delta_{mn}\varepsilon_{\psi}}{\iota - (n/m)}\,, \tag{61}$$

where $JG > 0$ and $\delta_{mn}\varepsilon_{\psi} > 0$ from the discussion above. In this limit A is determined by the sign of $(\iota - n/m)$. In a tokamak-like region where the toroidal curvature dominates, $n = 0$, increasing pressure gradient tends to make the average shear decrease. This limit corresponds to that considered in Ref. (10), where it was noted that for sufficiently large pressure gradient, the average shear changed from "stellarator-like" to "tokamak-like." In a region dominated by the helical curvature with $n > m\iota$, increasing pressure gradient makes the average shear larger. We note that this qualitative calculation can explain the behavior of the average shear observed in numerical calculations of high beta equilibria in the LHD configuration.[13,14] In the core region, the toroidal curvature dominates, while the helical curvature dominates in the outer parts of the plasma. As such, the shear is expected to decrease in the core and increase in the edge as the pressure gradient is built up.

The ballooning stability properties of currentless stellarators can also be understood by plotting the intersection of Eq. (57) with numerical solutions of the marginal ballooning equation, Eq. (49).

An alternative way to view the stability space of Mercier and ballooning modes is to plot them in a space parameterized by p' and σ. Using (33) to relate the average shear variation to the p' and σ variations, the Mercier stability diagram of Figure 1 is redrawn in Figure 2. In this plot, we assume $A > 0$ which

corresponds to a region dominated by a helical magnetic harmonic with $n > m\iota$. For this case, sufficiently large positive σ yields a Mercier stable region. Note, however, that this is in the opposite direction of the equilibrium bootstrap current caused by the magnetic field inhomogeneity with $n > m\iota$.[28] For regions with $A < 0$, the characteristic plot is inverted with a Mercier stable region for sufficiently negative equilibrium current which is opposite to the direction of the equilibrium bootstrap current. Clearly, the ballooning stability properties can be plotted in a space parameterized by p' and σ.

VI. Summary

In this work, the question of Mercier and ballooning stability in helical configurations is addressed by generalizing the work of Greene and Chance[12] to three-dimensional configurations. In this method, a set of equilibria are generated by imposing small amplitude variations of the plasma profiles on an initial arbitrary equilibrium. By demanding that the perturbed state is also an equilibrium, the profile variations are constrained so that only two free profile parameters describe the set. By using this method, one is able to characterize the stability properties of a particular magnetic surface by the use of a two-dimensional profile plot reminiscent of the s-α diagram used in tokamak stability studies.[4,12]

A particularly interesting limit is the currentless stellarator, where the set of equilibrium is parameterized by one free function, which can be chosen to be the pressure gradient. This set of equilibria is parameterized by a straight line in the more general two-dimensional stability plots. For this case, the Mercier stability of a magnetic surface is either always stable, or characterized by a first and second stability region at sufficiently low and high pressure gradient, respectively. Since the role of parallel currents in stellarators is an important

issue, we suggest an alternative way to view the more general stability space of a particular configuration is by using a p'-σ plot instead of the more commonly used p'-ι' plot.

As originally pointed out in Ref. (22), the eigenmode structure of ballooning modes in three-dimensional systems is more complicated than in axisymmetric tokamaks. In particular, due to the three-dimensionality of the stellarators, the eigenvalues are in general field line dependent. Because of this, there are two classes of eigenvalue level surfaces in the ballooning (ψ,θ_k,α) space, one describing topological cylinders which correspond to those of tokamak configurations and one describing topological spheres which are unique to stellarator configurations. It is suggested that by using the method for generating equilibria introduced in this work, one will be able to classify where the "cylindrical" and "spherical" ballooning eigenfunctions lie in the p'-ι' (or p'-σ) space. It has been speculated that the topologically sphere-shaped eigenvalue level surfaces are more localized in configurations space and hence more able to be stabilized by finite Larmor radius effects.[14] If the "spherical" ballooning modes are strongly stabilized by FLR, the stability space of the topologically cylindrical tokamak-like ballooning modes may provide a more practical beta limit in stellarators. We leave this topic for future theoretical investigation.

Acknowledgments

C. C. H. would like to thank the hospitality of the National Institute for Fusion Science in Nagoya, Japan where this research was carried out. C. C. H. would also like to thank J. N. Talmadge, J. D. Callen and the HSX research staff for a number of useful discussions and their continuing interest in this topic. The authors would also like to thank Prof. R. L. Dewar of the Australian National University for many interesting discussions and his interest in this work. This

work was primarily supported by the Japanese Ministry of Education, Science and Culture and in part by DOE grant no. DE-FG02-86ER53218.

Appendix: Variations in the magnetic coordinate

Variations in the magnetic coordinates are accounted for in the body of the paper by deriving relationships between the plasma profile shapes and the inverse coordinate mapping as described by (17), (27), (28) and (34). In this appendix we relate these variations to the magnetic coordinates in the varied equilibrium. As in GC, the changes in the profiles lead to shifting of the angle-like variables which are first order in μ, and shifts in the magnetic surfaces which are second order in μ.

The changes in θ and ζ at a given point in space will be calculated in terms of the initial equilibrium's magnetic coordinates. Namely, we write the perturbed coordinates

$$\theta = \theta^{(0)} + \mu\theta^{(1)} + \ldots \tag{A1}$$

$$\zeta = \zeta^{(0)} + \mu\zeta^{(1)} + \ldots \tag{A2}$$

$$\psi = \psi^{(0)} + \mu^2\psi^{(2)} + \ldots \tag{A3}$$

in terms of the initial coordinates and their variations, and calculate to first order the equation

$$\mathbf{x}(\psi,\theta,\zeta) = \mathbf{x}^{(0)}(\psi^{(0)},\theta^{(0)},\zeta^{(0)}) \ . \tag{A4}$$

This leads to the condition

$$\mathbf{x}^{(1)} + \theta^{(1)}\frac{\partial\mathbf{x}^{(0)}}{\partial\theta} + \zeta^{(1)}\frac{\partial\mathbf{x}^{(0)}}{\partial\zeta} = 0 \tag{A5}$$

which, using (27) and (28), leads to the conditions

$$\theta^{(1)} = \frac{-J\int dyD - \iota\int dy\beta^{(1)}}{(J + \iota I)} , \tag{A6}$$

$$\zeta^{(1)} = \frac{I\int dyD - \int dy\beta^{(1)}}{(J + \iota I)} , \tag{A7}$$

where I, J and ι are expressed in terms of their value in the initial equilibrium and the profile variations are expressed in terms of the variations $\beta^{(1)}$ and D, given in (25) and (34).

The variation $\psi^{(2)}$ can be derived from the equation

$$\frac{d^2\psi^{(2)}}{dy^2} = -\frac{d}{d\theta}\frac{d\theta^{(1)}}{dy} - \frac{d}{d\zeta}\frac{d\zeta^{(1)}}{dy} - \frac{1}{\sqrt{g}^{(0)}}\frac{d\sqrt{g}^{(1)}}{dy} , \tag{A8}$$

which results from accounting for first order variations in the Jacobian. It's straightforward to show this leads to the condition

$$\frac{d^2\psi^{(2)}}{dy^2} = -\frac{1}{\sqrt{g}(J+\iota I)}[(J\frac{\partial}{\partial\theta} - I\frac{\partial}{\partial\zeta})(D\sqrt{g}) + \frac{\partial}{\partial\eta}(\beta^{(1)}\sqrt{g})$$

$$+ \iota^{(1)}I + p^{(1)\prime}(2\sqrt{g} - V')] , \tag{A9}$$

where J, I and $\sqrt{g}$ are given by their value in the initial equilibrium.

References

1. S. Okamura, K. Matsuoka, K. Nishimura, K. Tsumori, R. Akiyama, S. Sakakibara, H. Yamada, S. Morita, T. Morisaski, N. Nakajima, K. Tanaka, J. Xu, K. Ida, H. Iguchi, E. Lazarus, T. Ozeki, H. Arimoto, A. Ejiri, M. Fujiwara, H. Ide, A. Iiyoshi, O. Kaneko, K. Kawahata, T. Kawamoto, A. Komori, S. Kubo, T. Kuroda, O. Motojima, V. D. Pustovitov, A. Sagara, C. Takahashi, K. Toi, and I. Yamada, in *Proceedings of the 15th International Conference on Plasma Physics and Contolled Nuclear Fusion Research*, Seville, 1994 (International Atomic Energy Agency, Vienna, 1995), Vol. 1, p. 381.
2. S. A. Sabbagh, R. A. Gross, M. E. Mauel, G. A. Navratil, M. G. Bell, R. Bell, M. Bitter, N. L. Bretz, R. V. Budny, C. E. Bush, M. S. Chance, P. C. Efthimion, E. D. Fredrickson, R. Hatcher, R. J. Hawryluk, S. P. Hirshman, A. C. Janos, S. C. Jardin, D. L. Jassby, J. Manickam, D. C. McCune, K. M. McGuire, S. S. Medley, D. Mueller, Y. Nagayama, D. K. Owens, M. Okabayashi, H. K. Park, A. T. Ramsey, B. C. Stratton, E. J. Synakowski, G. Taylor, R. M. Wieland, M. C. Zarnstorff, J. Kesner, E. S. Marmar, and J. L. Terry, Phys. Fluids B **3**, 2277 (1991).
3. J. R. Ferron, L. L. Lao, T. S. Taylor, Y. B. Kim, E. J. Strait, and D. Wroblewski, Phys. Fluids B **5**, 2532 (1993).
4. J. W. Connor, R. J. Hastie, and J. B. Taylor, Proc. R. Soc. London Ser. A **365**, 1 (1979).
5. R. L. Dewar, J. Manickam, R. C. Grimm, and M. S. Chance, Nucl. Fusion **21**, 493 (1981).
6. D. Correa-Restrepo, Z. Naturforsch **33a**, 789 (1978).
7. J. M. Greene and J. L. Johnson, Plasmas Phys. **10**, 729 (1968).
8. V. D. Shafarnov, Phys. Fluids **26**, 357 (1983).

9. H. L. Berk, M. N. Rosenbluth, and J. L. Shohet, Phys. Fluids **26**, 2616 (1983).

10. X. Llobet, H. L. Berk, and M. N. Rosenbluth, Phys. Fluids **30**, 2750 (1987).

11. W. A. Cooper, S. P. Hirshman, and D. K. Lee, Nucl. Fusion **29**, 617 (1989).

12. J. M. Greene and M. S. Chance, Nucl. Fusion **21**, 453 (1981).

13. N. Nakajima, Phys. Plasmas **3**, 4545 (1996).

14. N. Nakajima, Phys. Plasmas **3**, 4556 (1996).

15. W. A. Cooper, Phys. Plasmas **4**, 129 (1997).

16. J. Nührenberg and R. Zille, Phys. Lett. A **114**, 129 (1986).

17. W. A. Cooper, Y. Nakamura, M. Wakatani, R. Gruber, S. Merazzi, D. V. Anderson, and U. Schwenn, in *Proceedings of the 19th European Physical Society Conference on Controlled Fusion and Plasmas Physics*, Innsbruck, 1992 (European Physical Society, Petit-Lancy, 1992), ECA Vol. 10C, p. 557.

18. R. Moeckli and W. A. Cooper, Nucl. Fusion **33**, 1899 (1993).

19. W. A. Cooper and H. J. Gardner, Nucl. Fusion **34**, 729 (1994).

20. R. Moeckli and W. A. Cooper, Phys. Plasmas **1**, 793 (1994).

21. J. N. Talmadge and W. A. Cooper, Phys. Plasmas **3**, 3713(1996).

22. R. L. Dewar and A. H. Glasser, Phys. Fluids **26**, 3038 (1983).

23. W. A. Cooper, D. B. Singleton, and R. L. Dewar, Phys. Plasmas **3**, 275 (1996).

24. A. H. Boozer, Phys. Fluids **23**, 904 (1980).

25. A. Bhattacharjee, A. Hayashi, C. C. Hegna, N. Nakajima, and T. Sato, Phys. Plasmas **2**, 883 (1995) and references within.

26. A. H. Glasser, J. M. Greene, and J. L. Johnson, Phys. Fluids **18**, (1975).

27. A. H. Boozer, Phys. Fluids **24**, 1999 (1981).

28. A. H. Boozer and H. J. Gardner, Phys. Fluids B **2**, 2408 (1990).

Figure Captions

1. The Mercier stability space with $V^{tt} > 0$. The Mercier unstable region is that enclosed by the parabolic boundary described in Eq. (36). The lines correspond to the characteristic Mercier stability properties of a stellarator equilibrium with no net plasma current. The solid line that intersects the unstable region corresponds to $G > 0$. The dotted line corresponds a currentless equilibrium with $G < 0$.

2. Regions of Mercier stability plotted in a space parameterized by pressure gradient and equilibrium current. This plot corresponds to a magnetic surface where $A > 0$ or equivilantly a surface dominated by a magnetic harmonic with $n > m+$. This surface is stable to Mercier modes for sufficiently large equilibrium current. Below this characteristic value, Mercier modes are stable at sufficiently large and small pressure gradient.

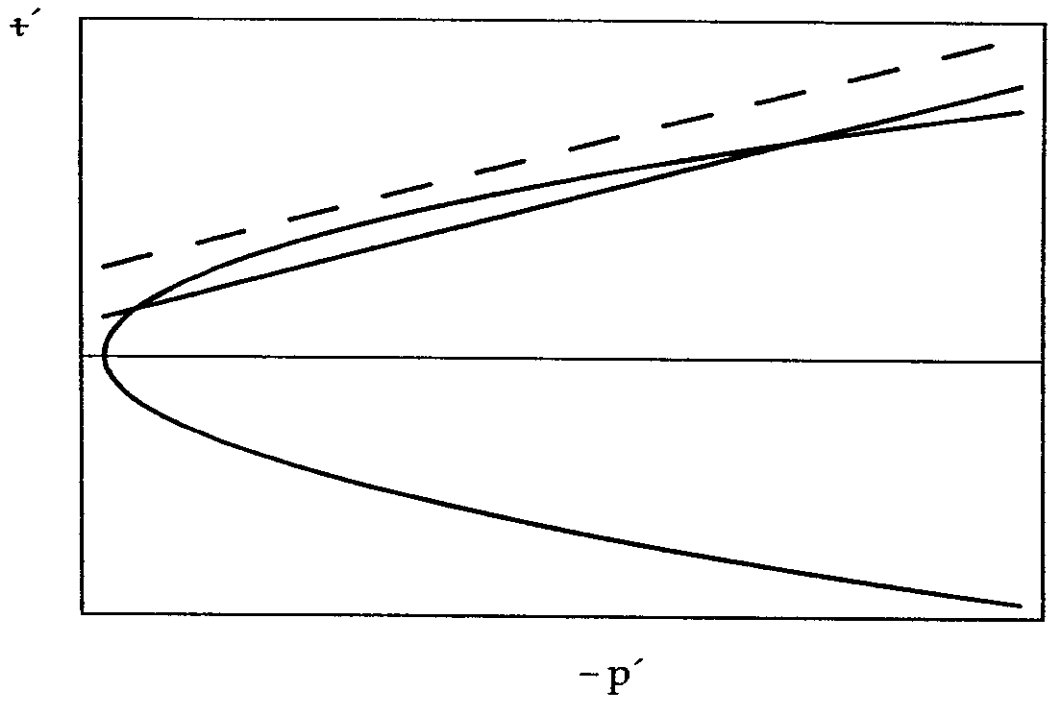

Fig. 1

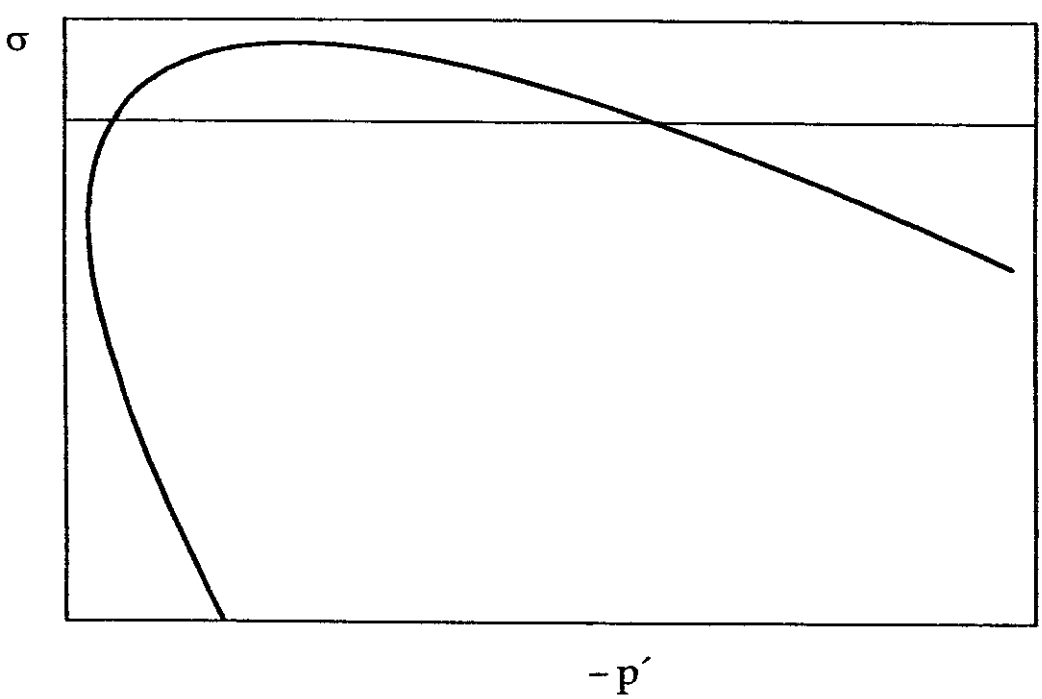

Fig. 2

Recent Issues of NIFS Series

NIFS-463 V. Voitsenya, V. Konovalov, O. Motojima, K. Narihara, M. Becker and B. Schunke,
Evaluations of Different Metals for Manufacturing Mirrors of Thomson Scattering System for the LHD Divertor Plasma; Nov. 1996

NIFS-464 M. Pereyaslavets, M. Sato, T. Shimozuma, Y. Takita, H. Idei, S. Kubo, K. Ohkubo and K. Hayashi,
Development and Simulation of RF Components for High Power Millimeter Wave Gyrotrons; Nov. 1996

NIFS-465 V.S. Voitsenya, S. Masuzaki, O. Motojima, N. Noda and N. Ohyabu,
On the Use of CX Atom Analyzer for Study Characteristics of Ion Component in a LHD Divertor Plasma; Dec. 1996

NIFS-466 H. Miura and S. Kida,
Identification of Tubular Vortices in Complex Flows; Dec. 1996

NIFS-467 Y. Takeiri, Y. Oka, M. Osakabe, K. Tsumori, O. Kaneko, T. Takanashi, E. Asano, T. Kawamoto, R. Akiyama and T. Kuroda,
Suppression of Accelerated Electrons in a High-current Large Negative Ion Source; Dec. 1996

NIFS-468 A. Sagara, Y. Hasegawa, K. Tsuzuki, N. Inoue, H. Suzuki, T. Morisaki, N. Noda, O. Motojima, S. Okamura, K. Matsuoka, R. Akiyama, K. Ida, H. Idei, K. Iwasaki, S. Kubo, T. Minami, S. Morita, K. Narihara, T. Ozaki, K. Sato, C. Takahashi, K. Tanaka, K. Toi and I. Yamada,
Real Time Boronization Experiments in CHS and Scaling for LHD; Dec. 1996

NIFS-469 V.L. Vdovin, T.Watari and A. Fukuyama,
3D Maxwell-Vlasov Boundary Value Problem Solution in Stellarator Geometry in Ion Cyclotron Frequency Range (final report); Dec. 1996

NIFS-470 N. Nakajima, M. Yokoyama, M. Okamoto and J. Nührenberg,
Optimization of M=2 Stellarator; Dec. 1996

NIFS-471 A. Fujisawa, H. Iguchi, S. Lee and Y. Hamada,
Effects of Horizontal Injection Angle Displacements on Energy Measurements with Parallel Plate Energy Analyzer; Dec. 1996

NIFS-472 R. Kanno, N. Nakajima, H. Sugama, M. Okamoto and Y. Ogawa,
Effects of Finite-β and Radial Electric Fields on Neoclassical Transport in the Large Helical Device; Jan. 1997

NIFS-473 S. Murakami, N. Nakajima, U. Gasparino and M. Okamoto,
Simulation Study of Radial Electric Field in CHS and LHD; Jan. 1997

NIFS-474 K. Ohkubo, S. Kubo, H. Idei, M. Sato, T. Shimozuma and Y. Takita,

Coupling of Tilting Gaussian Beam with Hybrid Mode in the Corrugated Waveguide; Jan. 1997

NIFS-475 A. Fujisawa, H. Iguchi, S. Lee and Y. Hamada,
Consideration of Fluctuation in Secondary Beam Intensity of Heavy Ion Beam Prove Measurements; Jan. 1997

NIFS-476 Y. Takeiri, M. Osakabe, Y. Oka, K. Tsumori, O. Kaneko, T. Takanashi, E. Asano, T. Kawamoto, R. Akiyama and T. Kuroda,
Long-pulse Operation of a Cesium-Seeded High-Current Large Negative Ion Source; Jan. 1997

NIFS-477 H. Kuramoto, K. Toi, N. Haraki, K. Sato, J. Xu, A. Ejiri, K. Narihara, T. Seki, S. Ohdachi, K. Adati, R. Akiyama, Y. Hamada, S. Hirokura, K. Kawahata and M. Kojima,
Study of Toroidal Current Penetration during Current Ramp in JIPP T-IIU with Fast Response Zeeman Polarimeter; Jan., 1997

NIFS-478 H. Sugama and W. Horton,
Neoclassical Electron and Ion Transport in Toroidally Rotating Plasmas; Jan. 1997

NIFS-479 V.L. Vdovin and I.V. Kamenskij,
3D Electromagnetic Theory of ICRF Multi Port Multi Loop Antenna; Jan. 1997

NIFS-480 W.X. Wang, M. Okamoto, N. Nakajima, S Murakami and N. Ohyabu,
Cooling Effect of Secondary Electrons in the High Temperature Divertor Operation; Feb. 1997

NIFS-481 K. Itoh, S.-I. Itoh, H. Soltwisch and H.R. Koslowski,
Generation of Toroidal Current Sheet at Sawtooth Crash; Feb. 1997

NIFS-482 K. Ichiguchi,
Collisionality Dependence of Mercier Stability in LHD Equilibria with Bootstrap Currents; Feb. 1997

NIFS-483 S. Fujiwara and T. Sato,
Molecular Dynamics Simulations of Structural Formation of a Single Polymer Chain: Bond-orientational Order and Conformational Defects; Feb. 1997

NIFS-484 T. Ohkawa,
Reduction of Turbulence by Sheared Toroidal Flow on a Flux Surface; Feb. 1997

NIFS-485 K. Narihara, K. Toi, Y. Hamada, K. Yamauchi, K. Adachi, I. Yamada, K. N. Sato, K. Kawahata, A. Nishizawa, S. Ohdachi, K. Sato, T. Seki, T. Watari, J. Xu, A. Ejiri, S. Hirokura, K. Ida, Y. Kawasumi, M. Kojima, H. Sakakita, T. Ido, K. Kitachi, J. Koog and H. Kuramoto,
Observation of Dusts by Laser Scattering Method in theJIPPT-IIU Tokamak

Mar. 1997

NIFS-486 S. Bazdenkov, T. Sato and The Complexity Simulation Group,
Topological Transformations in Isolated Straight Magnetic Flux Tube; Mar. 1997

NIFS-487 M. Okamoto,
Configuration Studies of LHD Plasmas; Mar. 1997

NIFS-488 A. Fujisawa, H. Iguchi, H. Sanuki, K. Itoh, S. Lee, Y. Hamada, S. Kubo, H. Idei, R. Akiyama, K. Tanaka, T. Minami, K. Ida, S. Nishimura, S. Morita, M. Kojima, S. Hidekuma, S.-I. Itoh, C. Takahashi, N. Inoue, H. Suzuki, S. Okamura and K. Matsuoka,
Dynamic Behavior of Potential in the Plasma Core of the CHS Heliotron/Torsatron; Apr. 1997

NIFS-489 T. Ohkawa,
Pfirsch - Schlüter Diffusion with Anisotropic and Nonuniform Superthermal Ion Pressure; Apr. 1997

NIFS-490 S. Ishiguro and The Complexity Simulation Group,
Formation of Wave-front Pattern Accompanied by Current-driven Electrostatic Ion-cyclotron Instabilities; Apr. 1997

NIFS-491 A. Ejiri, K. Shinohara and K. Kawahata,
An Algorithm to Remove Fringe Jumps and its Application to Microwave Reflectometry; Apr. 1997

NIFS-492 K. Ichiguchi, N. Nakajima, M. Okamoto,
Bootstrap Current in the Large Helical Device with Unbalanced Helical Coil Currents; Apr. 1997

NIFS-493 S. Ishiguro, T. Sato, H. Takamaru and The Complexity Simulation Group,
V-shaped dc Potential Structure Caused by Current-driven Electrostatic Ion-cyclotron Instability; May 1997

NIFS-494 K. Nishimura, R. Horiuchi, T. Sato,
Tilt Stabilization by Energetic Ions Crossing Magnetic Separatrix in Field-Reversed Configuration; June 1997

NIFS-495 T. -H. Watanabe and T. Sato,
Magnetohydrodynamic Approach to the Feedback Instability; July 1997

NIFS-496 K. Itoh, T. Ohkawa, S. -I.Itoh, M. Yagi and A. Fukuyama
Suppression of Plasma Turbulence by Asymmetric Superthermal Ions; July 1997

NIFS-497 T. Takahashi, Y. Tomita, H. Momota and Nikita V. Shabrov,
Collisionless Pitch Angle Scattering of Plasma Ions at the Edge Region of an FRC; July 1997

NIFS-498 M. Tanaka, A.Yu Grosberg, V.S. Pande and T. Tanaka,
Molecular Dynamics and Structure Organization in Strongly-Coupled Chain of Charged Particles; July 1997

NIFS-499 S. Goto and S. Kida,
Direct-interaction Approximation and Reynolds-number Reversed Expansion for a Dynamical System; July 1997

NIFS-500 K. Tsuzuki, N. Inoue, A. Sagara, N. Noda, O. Motojima, T. Mochizuki, T. Hino and T. Yamashina,
Dynamic Behavior of Hydrogen Atoms with a Boronized Wall; July 1997

NIFS-501 I. Viniar and S. Sudo,
Multibarrel Repetitive Injector with a Porous Pellet Formation Unit; July 1997

NIFS-502 V. Vdovin, T. Watari and A. Fukuyama,
An Option of ICRF Ion Heating Scenario in Large Helical Device; July 1997

NIFS-503 E. Segre and S. Kida,
Late States of Incompressible 2D Decaying Vorticity Fields; Aug. 1997

NIFS-504 S. Fujiwara and T. Sato,
Molecular Dynamics Simulation of Structural Formation of Short Polymer Chains; Aug. 1997

NIFS-505 S. Bazdenkov and T. Sato
Low-Dimensional Model of Resistive Interchange Convection in Magnetized Plasmas; Sep. 1997

NIFS-506 H. Kitauchi and S. Kida,
Intensification of Magnetic Field by Concentrate-and-Stretch of Magnetic Flux Lines; Sep. 1997

NIFS-507 R.L. Dewar,
Reduced form of MHD Lagrangian for Ballooning Modes; Sep. 1997

NIFS-508 Y.-N. Nejoh,
Dynamics of the Dust Charging on Electrostatic Waves in a Dusty Plasma with Trapped Electrons; Sep.1997

NIFS-509 E. Matsunaga. T.Yabe and M. Tajima,
Baroclinic Vortex Generation by a Comet Shoemaker-Levy 9 Impact; Sep. 1997

NIFS-510 C.C. Hegna and N. Nakajima,
On the Stability of Mercier and Ballooning Modes in Stellarator Configurations; Oct. 1997